Surface Molecule Manipulated Pt/TiO_2 Catalysts for Selective Hydrogenation of Cinnamaldehyde

Ran Tao, [1#] Bing-Qian Shan, [#*1] Hao-Di Sun, [1] Meng-Ding, [1] Qing-Song Xue,[1] Jin-Gang Jiang, [1] Peng Wu, [1*] Kun Zhang[1,2*]

[1] Shanghai Key Laboratory of Green Chemistry and Chemical Processes, Laboratory of Interface and Water Science, College of Chemistry and Molecular Engineering, East China Normal University, Shanghai 200062, China;

[2] Shandong Provincial Key Laboratory of Chemical Energy Storage and Novel Cell Technology, School of Chemistry and Chemical Engineering, Liaocheng University, Liaocheng, 252059, Shandong, P. R. China.

*Correspondence:bqshan_ecnu@163.com, kzhang@chem.ecnu.edu.cn, pwu@chem.ecnu.edu.cn

Abstract

Surface states—the electronic states arising as a result of the different bonding environment—are easily contaminated by adsorbed molecules at nanoscale interfaces of metal nanoparticles (NPs), which generally poison the active sites of heterogeneous catalysts. Herein, we use selective hydrogenation of cinnamaldehyde (CAL) on platinum-covered titanium oxide (Pt@P25) as a prototype reaction, and show that the competitive exchange of extra-introduced species (sodium hydroxide and sodium formate) with spontaneously formed weak bound carbonate and bicarbonate anions at Pt NPs can reconstruct the surface states, which directs the preferred adsorption of the conjugated C=O and C=C double bonds of CAL, and consequently, results in highly efficient synthesis of unsaturated alcohol cinnamyl alcohol (COL) and saturated aldehyde hydrocinnamaldehyde (HCAL) with high selectivity of 94.7% and 97.6%, respectively. Our concept of restructured surface states to tune the chemoselectivity of α, β-unsaturated aldehydes triggered by the selective adsorption of alien molecules may lead to new design principles of heterogeneous catalysts, beyond the conventional d-band theory.

Introduction

The catalytic selective hydrogenation of cinnamyl aldehyde (CAL) is of pivotal reaction in both academic and industrial fields (*1*, *2*). Owing to the close bond energy between the conjugated C=O and C=C double bonds, selective synthesis of pure single product of cinnamyl alcohol (COL) and hydrocinnamaldehyde (HCAL) is still a formidable challenge. Previous attempts to improve the chemoselectivity of metal nanocatalysts mainly focused on controlling the size, shape and composition of metal NPs, and, the interactions between metal and supports (*1-6*). More recent researches have seen an increased focus on understanding the interactions between adsorbates at nanoscale interfaces of heterogeneous catalysts (*7-24*). But, how these interactions

can be precisely regulated to tune the chemical reactivity remains elusive.

Generally, the increased selectivity comes at the expense of reaction activity, due to the site blocking effects caused by interaction of reactive sites with adsorbates (*12, 25, 26*). However, in some cases, simultaneous enhancements of selectivity and activity in metal catalysts modified by electron-rich heteroatomic were observed (*8, 27-29*), even in non-metal heteroatomic catalysts (*30, 31*), suggesting a new reaction channel to chemoselective redox chemistry at metal nanoscale interface. Very recently, after long-term and systematic investigation, using a combined experimental and computational approach, in particular with the help of steady and ultra-fast absorption and emission spectrum, we unambiguously confirmed the existence of new interface states due to the spatial overlapping of p orbitals of surface ligand atoms on the surface of metal nanoclusters (NCs) (*32-41*). It is called p band intermediate state (PBIS), which not only provides an ensemble of intermediate states for bright photoluminescence (PL) emission, but also acts as an alternative reaction channel for static electron transfer. Our preliminary results on the testing of catalytic hydride reduction of $–NO_2$ to NH_2 by constructing the surface states with adsorbates on metal surface (*40, 41*), based on the principle of new conceptual of PBIS model, is maybe feasible for the selective hydrogenation of α,β-unsaturated aldehydes.

Herein, we present a comprehensive study of CAL hydrogenation on a series of Pt@P25 catalysts with a delicate change of interface states triggered by the adsorptions of very simple organic and inorganic additives, such as sodium formate (HCOONa), sodium acetate (CH_3COONa), sodium methoxide (CH_3ONa) and NaOH. Upon the introduction of HCOONa, almost 100% of HCAL product was collected through the selective hydrogenation of the C=C groups with an expectedly average conversion efficiency of ca. 15.6% owing to the blocking of catalytic active sites by strongly bound $HCOO^-$ anions on Pt NPs surface. At identical reaction conditions, when other organic sodium salts (CH_3COONa or CH_3ONa) were introduced, the COL product via selective hydrogenation of C=O groups was favorably obtained with maximum conversion (92.6%) and selectivity (95.4%), much higher than that of parent catalyst free any additives (conversion less than 90% and selectivity less than 20%), and very interestingly the conversion and selectivity shows pH dependence. The observation of Fourier transform infrared spectroscopy (FT-IR) shows that, CH_3ONa organic additives are not adsorbed on Pt NPs due to the competitive adsorption of hydroxide groups, which originates from the ionization of organic additives with a feature of weak acid. Combined with the characterization of optical spectroscopy, a designed diagnostic experiment, i.e., the introduction of NaOH as inorganic additives significantly promoting the selective hydrogenation of C=O groups, further evidences the key role of surface hydroxyl to construct the surface state to tune the chemical reactivity. We anticipate that our molecularly manipulated surface state restructuring strategy towards selective hydrogenation of the conjugated C=O and C=C double bonds will allow the development of other selective heterogeneous catalysts with different types of metals and supports for important yet challenging transformations.

Result and Discussion

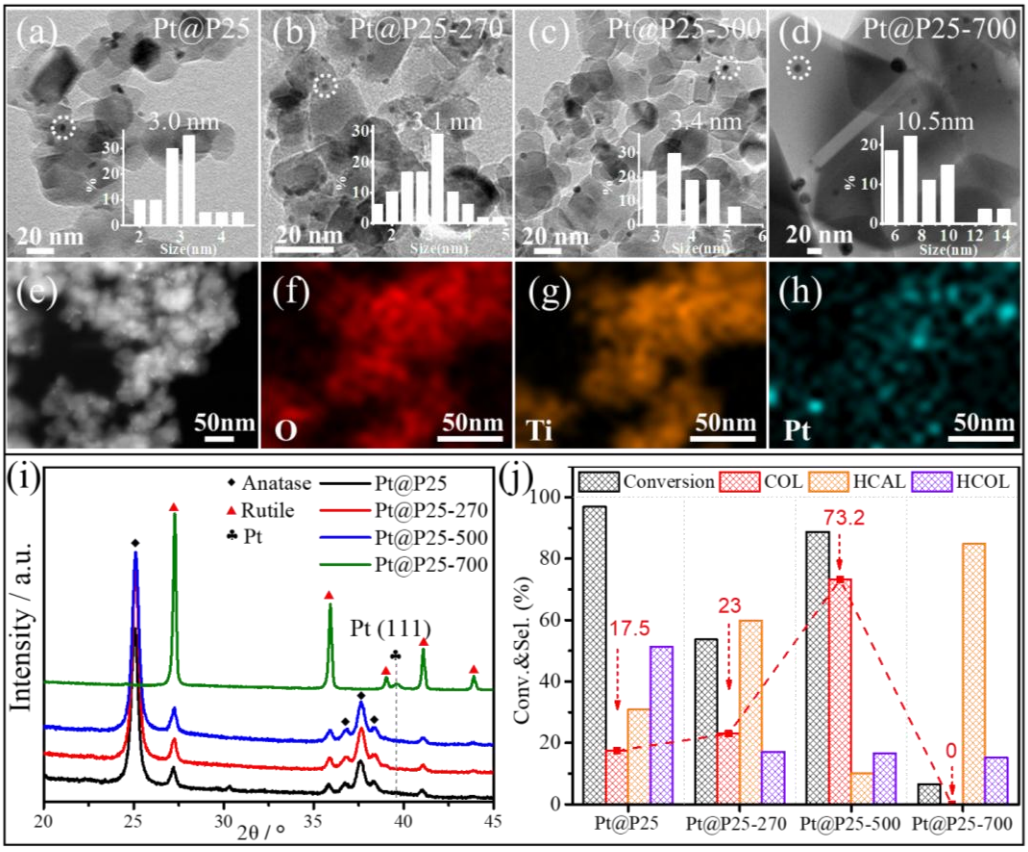

Figure 1 | TEM images of Pt@P25 (a), Pt@P25-270 (b), Pt@P25-500 (c) and Pt@P25-700 (d). The inset is the corresponding particle size distribution. HAADF-STEM image (e) and EDX elemental analysis (f-h) of Pt@P25-500 catalyst. XRD patterns (i) and catalytic reactivity (j) of Pt@P25 and Pt@P25-T (T=270, 500, 700℃).

Pt-based catalysts (Pt@P25) with 2 wt % Pt loading were prepared via the simple impregnation method with sodium borohydride ($NaBH_4$) as a reducer and commercial P25 as a support (Experiment section in Supporting Information). The combined characterizations by the transmission electron microscopy (TEM) (Fig. 1a), annular dark-field TEM (Fig. 1e) and corresponding elemental mapping (Fig. 1f-1h), and XRD (Fig. 1i) confirmed that the Pt NPs are nanometer in size of ca. 3.0 nm and uniformly distributed throughout P25 nanoparticles. Take account of the well-known characteristic of noble metal NPs deposited TiO_2 that carbonaceous species are fairly easily to contaminate the surface once exposed in the air (*42*, *43*), which blocks the catalytic active sites, consequently resulting in the low activity of catalysts. This was confirmed by our FT-IR observation and TG analysis (Fig. 3). To remove the surface contaminates, two groups of Pt@P25 catalysts were prepared by high-temperature calcinations at T=270, 500, 700℃, which were denoted as Pt@P25-T and Pt@(P25-T), respectively. Pt@P25-T means that Pt NP deposited P25 was calcined at varied temperatures. Pt@(P25-T) means that parent P25 support was calcined at varied temperatures before Pt NPs deposition.

The observation of TEM shows that, only when the calcination temperature is larger than 500°C, the size of Pt NPs is significantly increased from ca. 3.0 nm to 10.5

nm (Fig. 1a-1d), concomitantly companying a full transform of crystal structure from anatase (W_A) to rutile (W_R) due to high-temperature restructuring, which was confirmed by the characterization of XRD patterns (Fig. 1i). A very interesting result is observed, in the presence of Pt metals, anatase (W_A) was almost full transformed rutile (W_R) phase, which was never reported before, but beyond the scope of this research. Surprisingly, the chemical reactivity of cinnamaldehyde hydrogenation displayed a completely different temperature-dependent behavior (Fig. 1j): With the increase of calcination temperature, the conversion rate of the reaction was first reduced (53.7%), then increased (88.8%), and then decreased again (6.6%). Obviously, the very low conversion of Pt@P25 at 700°C is assigned to the inert Pt NPs with larger size due to Ostwald ripening growth. But we cannot completely preclude the influence of crystal structure of P25 on chemical reactivity. To address this point, before the Pt NPs deposition, the P25 support was first treated by high-temperature calcination. This series of catalysts are named Pt@(P25-T). The results of reaction performance shows in figure 2b that, the conversion of Pt@(P25-T) was decreased to ca.85%, compared with parent catalyst of Pt@P25 (97.0%), while the selectivity was not significantly changed (ca. 17.0%) with the temperature increase from 270 to 700°C, even though the mass fraction of rutile (W_A) were effectively tuned from 80.4% in Pt@(P25-270) to 41.9% in Pt@(P25-700) (Figure 2a, Table S1). These results indicate that the catalytic performance of selective hydrogenation of CAL on Pt@P25 is independent on the crystals structure, i.e., the mass ratio of W_A/W_R.

Compared to Pt@P25, even though the conversion of Pt@P25-500 was decreased from 97.0% to 88.8%, the selectivity on COL was significantly increased from 17.5% to 73.2% (Fig. 1j). Since both catalysts have almost the same size of Pt NPs (ca. 3.0 nm, Fig. 1a, 1c) and structural composition of P25 (W_A/W_R = 4.0, Fig. 1i and Table S1), the great difference on the hydrogenation selectivity is presumably attributed to the delicate change of interface microenvironment of Pt NPs catalytic sites, which is caused by removal of surface adsorbates by the high-temperature calcination. Combined characterizations by Fourier transform infrared spectroscopy spectrum (FT-IR), thermalgravity and differential thermalgravity analysis (TG-DTG), and thermalgravity-Mass spectrometer (TG-MASS) confirmed this point.

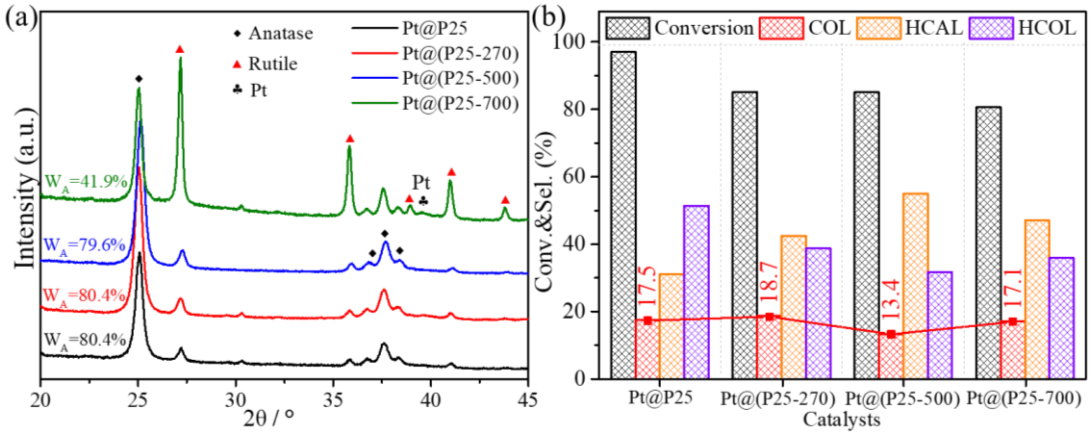

Figure 2 | XRD patterns (a) and catalytic reactivity (b) of Pt@P25, Pt@(P25-T) (T=270, 500, 700℃).

On the FT-IR spectrum (Fig. 3a and 3b), the P25 support just showed an adsorption bands centered at ca. 1635 cm^{-1}, which is attributed to the bent vibration of hydroxyl groups from surface titanol (Ti-OH) or adsorbed hydroxide and water molecules at coordinatively unsaturated (cus) Ti centers. When Pt NPs were deposited on P25 support, due to the binding and subsequent activation of Pt NPs on the CO_2 molecules in the air atmosphere, typical fingerprint bands to carbonate species in a very broad range from 900 to 1800 cm^{-1} were observed (Table S3), which are mainly attributed to bidentate carbonate groups (bands at 1032, 1345 and 1574 cm^{-1}) and bicarbonate species (bands at 1220, 1411 and 1636 cm^{-1}). Generally, the surface bidentate carbonate species are formed involving the interaction with Lewis acid–base pairs sites (cus Ti^{4+}-O^{2-} centers), and the bicarbonate species are produced by a reaction of CO_2 with basic OH groups (*44-48*). Obviously, the formation of interfacial layer of carbonaceous species on Pt NPs blocked the preferential absorption of C=O of CAL, which promoted the selective hydrogenation of C=C double bonds with selectivity larger than 50% (Fig. 1j and Fig. 2b). When calcination temperature was increased to 270^{o}C, the surface carbonate species of both Pt@P25-270 and Pt@P25-500 catalysts were clearly removed since only surface hydroxyl groups are observed at ca. 1635 cm^{-1} (Fig. 3a and 3b), as observed for parent P25 support. It is importantly noted that, even these two catalysts had the similar interface microenvironments, they showed completely different catalytic hydrogenation behaviors of C=C (ca. 59.9%) and C=O (ca. 73.2%) double bonds for Pt@P25-270 and Pt@P25-500 (Fig. 1j), suggesting not only the nature but also the coverage degree (or density) of surface hydroxyl groups determine the final chemical reactivity. If further increasing calcination temperature up to 700^{o}C, we surprise find that, besides the bidentate carbonate and bicarbonate species, additional mono-dentate carbonate species were regenerated with typical absorbance bands at 1468 and 1382 cm^{-1} (Fig. 3b and Table S3), which probably results in the full selective transformation of CAL to HCAL, i.e, the preferred hydrogenation of C=C bond (Fig. 1j), further suggests the delicate change of surface microenviroment of active sites significantly affects the catalytic performances.

TG-DTG analysis confirms these assignments of surface adsorbed species (Fig. 3c and 3d). For Pt@P25 and Pt@P25-700, two apparent weightlossness peaks were observed at around 120 ℃ and 260 ℃ with total weightloss of 5.6% and 3.7%, respectively. However, for Pt@P25-270 and Pt@P25-500, besides the weight loss of physically adsorbed water at less than 100^{o}C, only one main peak of weightloss of was found at 260^{o}C, which is assigned to the surface hydroxyl groups, and their total weightloss of about 2.3% is much less than that of Pt@P25 and P25 support. The TG-Mass (Fig. S2) exhibits stronger evidence that the wightloss at 120 ℃ and 260 ℃ is assigned to the decomposition of carbon species and departure of water molecules by the reaction of surface hydroxyl groups because of the detection of gas CO_2 and water molecules on corresponding decomposition temperature, respectively. Similar carbon species also observed for Pt@(P25-T) series catalysts, but they don't show the temperature dependent evolution behavior, indicating that, Pt NPs are active sites for CO_2 activation, innocent to the structure of P25 support (Fig. S1 and S3). This also answers that the catalytic activity of Pt@(P25-T) series catalysts is independent on the

calcination temperature of P25 (Fig. 2b). Taken all the data together, we concludes that the carbon species are weakly bounded on the surface of Pt NPs since they are very easily desorbed or decomposed at very low calcination temperature (less than 150°C), and that, importantly, the nature of adsorbates determines the chemical reactivity and chemoselectivity of final products, i.e, the carbonate species and hydroxyl groups promote the selective hydrogenation of C=C and C=O double bond of CAL, respectively. However, after high-temperature calcination treatment, the transformation of C=O functions was only about 73.2% (Fig. 1j), which is much less than expected value for practical applications.

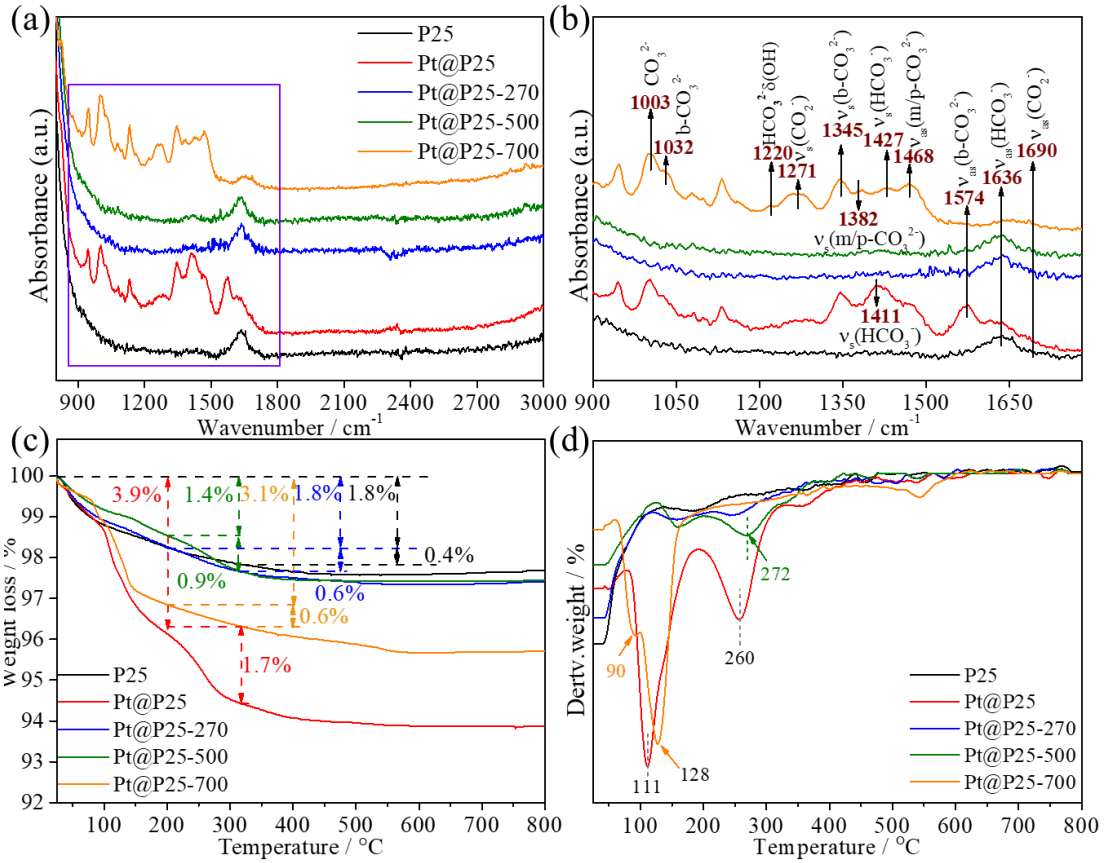

Figure 3. | FT-IR spectra of P25, Pt@P25 and Pt@P25-T (T=270, 500, 700℃) (a). And (b) is a larger version of the purple rectangle in (a). TG-DTG curves of Pt@P25-T (T=270, 500, 700℃) (c, d).

Inspired by this discovery, we performed the detailed investigation of the effects of small organic molecules on selective hydrogenation of CAL on Pt@P25 catalyst, including sodium formate (HCOONa), sodium acetate (CH_3COONa) and sodium methoxide (CH_3ONa), in particular for HCOONa owing to its key intermediate role for the activation of C1 chemistry. To our surprise, three organic additives show completely different catalytic performance (Fig. 4a): upon the introduction of HCOONa, Pt@P25 showed a decreased conversion rate (15.6%) for the hydrogenation of CAL, but an almost full transformation of CAL to HCAL with the selectivity of C=C hydrogenation (ca. 100%); However, when CH_3COONa and CH_3ONa were introduced, a favored hydrogenation of C=O double bonds was achieved with conversion (75.5%) and high selectivity (59.5%), and amazingly in the case of CH_3ONa, the conversion and selectivity of CAL to COL had reached 92.6%

and 95.4%, respectively. To reveal the influence of organic additive adsorption on the catalytic performance, FT-IR spectra of the catalysts after reaction was carried out (Figure 4b). Compared with unreacted catalyst Pt@P25 (Figure 4b, black line), after reaction, surface carbon species could be completely removed from the catalyst surface (Figure 4b, red line), once again confirming that carbonate and bicarbonate anions are weakly bounded on Pt/TiO_2 interfaces as observed by TG (Fig. 3a and 3b). When HCOONa and CH_3COONa was added, a strongly adsorbed band at 1670 cm^{-1} was observed, which is attributed to the fingerprint vibration of carboxylate functions in HCOONa and CH_3COONa due to its strong coordination ability with Pt metals (*45, 49*). The blocking of Pt active sites by saturated adsorbed $HCOO^-$ anions after adding HCOONa also answers the low chemical reactivity with a conversion of 15.6% (Fig. 4a). Very interestingly, the adsorption CH_3COONa shows the medium conversion rate (ca. 78%), but a relative high selectivity for C=O hydrogenation (ca. 60%).

However, when CH_3ONa was introduced, we do not observe any adsorption of organic additive itself. In turn, interestingly three easily distinguished adsorption bands centering at 1440, 1557and 1639 cm^{-1} were observed with broader full width at half maximum (FWHM), which were different from the carbonate and bicarbonate species, but having some common features (Fig. 4b, pink line). It should be mentioned that, due to the weak acid and strong alkali characteristics of CH_3COONa and CH_3ONa, their reaction solution showed high pH value (8.25 and 12.45, Table S2). Considering the stronger interaction between hydroxide and Pt NPs, OH^- hydrolyzed from weak acid salts will prefer adsorbing on the Pt NPs surface, and its saturation degree determines the chemical activity and selectivity. In the case of CH_3COO^- (lower pH produces less OH^-), because of competitive adsorption between OH^- and CH_3COO^-, the surface of Pt NPs was only partial covered by OH^-, thus the medium conversion rate (ca. 78%), but a relative high selectivity for C=O hydrogenation (ca. 60%) for CAL transformation was achieved (Fig. 4a) The direct introduction of NaOH as a diagnostic experiment to further confirm the pivotal role of saturated adsorbed surface hydroxyl groups to regulate the chemical reactivity, almost full conversion and single selectivity were reached when NaOH was introduced (Fig. 4a). It is importantly noted that, the selective hydrogenation of CAL to COL was not only applicable for titania, but also for silica support (item 5 and 6 in the Table S2), further suggesting the improvement of selectivity is independent on the type and structure of supports (Fig. 2). Thus, several critical questions are naturally coming as follows: why does the very delicate change of interface environment of catalytic sites, i.e., very similar chemical structures of adsorbed carbonate species (Fig. 4b), makes a great change for CAL selective transformation; why do the surface carbonate and/or bicarbonate adsorbates benefit to the formation of HCAL (C=C hydrogenation), while surface adsorbed hydroxyl-CO_2 complex promote the C=O hydrogenation (Fig. 1j and Fig. 4a); what is the nature of hydroxyl-CO_2 complex at nanoscale interface, especially in the presence of NaOH; and whether there are ubiquitous surface states at Pt NPs to tune chemical reactivity?

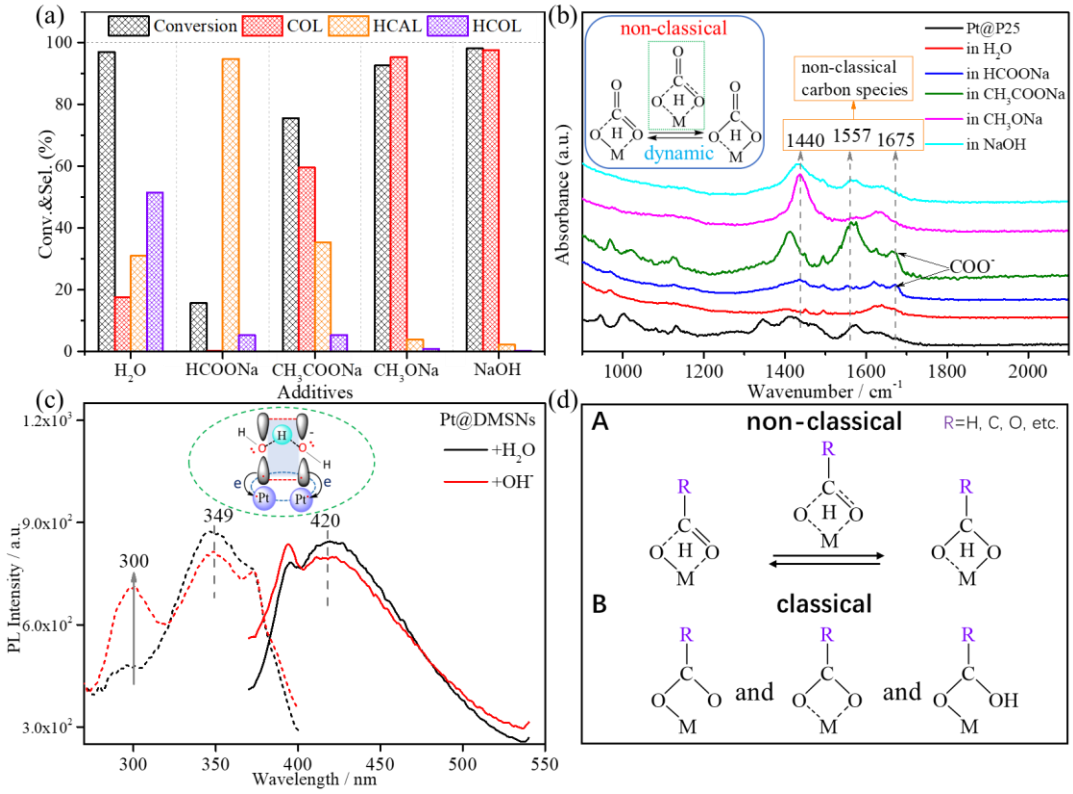

Figure 4. | (a) The reactivity of cinnamaldehyde hydrogenation without (H_2O) or with different additives in Pt@P25 catalyst. (b) FT-IR spectra of the catalysts after reaction. (b) Excitation (dash line) and emission spectra (solid line) of Pt@DMSNs in H_2O (black line) and NaOH (1M) (red line). (d) Proposed carbon-oxygen species structures.

Very recently, p band intermediate states (PBIS) with the characteristic of a $\pi \rightarrow \pi^*$ transition, which is formed through space interactions of p orbitals of paired O atoms in a hydrated hydroxide intermediate $[X^+ \bullet (OH^- \bullet H_2O)(H_2O)_{n-1}]$, were captured by a steady and ultrafast transient absorption spectrum in picosecond (ps) scale (*35-37*). These dynamic surface states provide more alternative reaction channels for concerted electron and proton transfer, which promotes the conversion and selectivity of chemical transformations beyond the conventional d band theory (*40, 41*). Note that, here unfortunately, due to the interfering of intrinsic luminescent properties of defect states in TiO_2 semiconductors with surface states of adsorbate species, we cannot directly use Pt@P25 to investigate the nature of surface states. But we know that, the catalytic properties of Pt NPs is independent on the type and structure of supports as we discussed above (Table S2), Pt@DMSNs catalyst with nonlumniscent silica is an ideal support to investigate the nature of interface state by following its luminescent properties. In our previous reports, we have already established the solid correlation between interface states and PL emissions (*35-38, 40*).

The observation of excitation and PL spectrum (Fig. 4c) of Pt@DMSNs catalysts proves the presence of surface states, and they are strongly dependent on the delicate change of interface microenvironment. Pt@DMSNs in both water and NaOH solution shows strong PL emissions at ca. 390 nm and ca. 420 nm under the UV irradiation at 360 nm, which corresponded to the excitation bands at ca. 300 nm and 349 nm,

respectively. But, in basic solution, the emission at 395 nm was greatly intensified, concomitantly producing a strong adsorption at 300 nm on excitation spectrum (Fig. 4c, red line). Since Pt NPs is non-luminescent metal, the origin of PL of Pt NPs is attributed to the electron transition of surface states, which is formed due to the p orbital overlapping of paired O atoms in surface hydrous hydroxide complex (also called structural water molecule with symmetrical hydrogen-bond interaction) though space interaction.

These unique surface states determined the adsorption characteristics and chemical structures of CO_2, i.e., consequently the selective transformation of CAL. In the absent of OH^-, the classical carbonate species (Fig. 4d), which was formed by a direct chelating interaction of transition metal and CO_2 from air atmosphere, including bidentate, monodentate or bicarbonate species, were weakly bounded on the Pt@P25 interface (Scheme 1i). When HCOONa with strong chelating ability to Pt NPs was introduced, a dense formate layer was covered on the surface of Pt active sites (Scheme 1 ii), which not only blocked the access of CAL molecules, but also prohibited the preferred adsorption of C=O functions (Scheme 1 iii). Therefore, the product of HCAL with preferred selective hydrogenation of C=C double bond (~100%) was collected in relatively low conversion rate. Upon the introduction of hydroxide anions (NaOH and CH_3ONa), due to the stronger coordination interaction of OH^- with Pt metal, a monolayer of hydrous hydroxide complex (or structural water molecules) was strongly covered on the surface of Pt NPs (Scheme 1, iv), where an ensemble of interface states (PBIS states) was formed by the spatial overlapping of p orbitals of oxygen atoms (scheme 1, inset, green circle iv). Due to the strong binding of OH^- to Pt NPs, the direct coordination interaction of CO_2 with metal surface was blocked, thus classical carbonate species cannot be formed (Fig. 3b and Fig. 4 d). But, a new metastable hydroxyl-CO_2 complex is formed, completely differing from the classical carbonate species, herein, we call it non-classical carbonate species (Fig. 4b and 4d).

The non-classical carbonate species were postulated to form by nucleophilic attack of surface hydroxyl on carbon atom of CO_2. Its structure was not stable as classical carbonate species, and it can be depicted in 3c-2e and π complex formulations as discovered in 2-norbornyl cation (Fig. 4b, inset) (*50*). Its dynamical structure answers the broadening of adsorption bands on FT-IR spectrum, compared to the classical carbonate species (Fig. 4b). During the selective hydrogenation of CAL, due to the metastable feature of non-classical carbonate structure, CO_2 can be readily exchanged by carbonyl group of CAL reactant (Scheme1v, inset in green circle, and Fig. 4d), concomitantly C=O double bond of CAL are activated, thus COL with high selectivity (>95%) and conversion (>95%) is collected over the thermo-dynamical limitation of unfavored C=O hydrogenation.

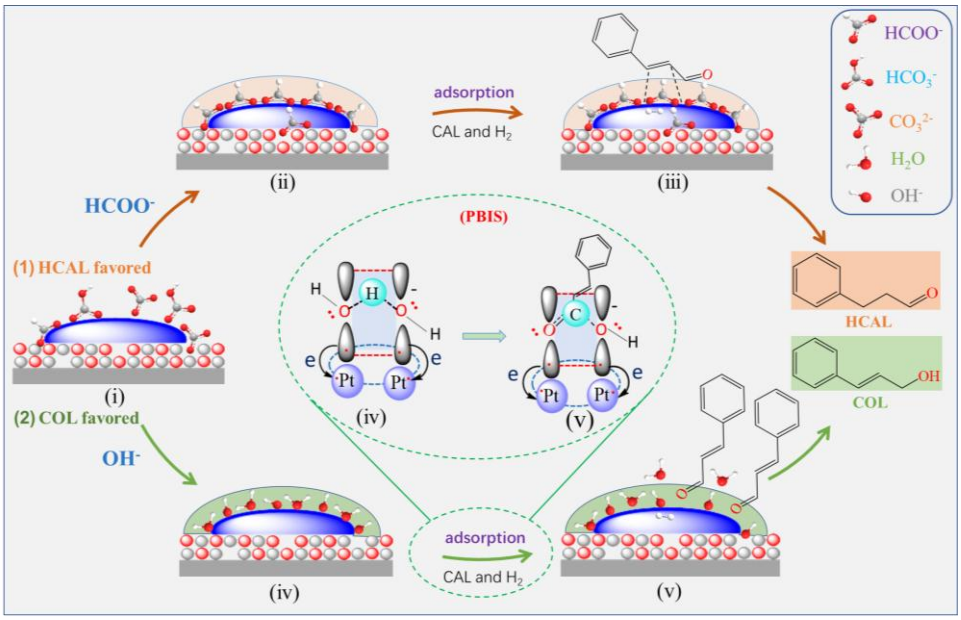

Scheme 1. | Proposed mechanism and reaction routes (green arrows: COL-favored route; red arrows: HCAL-favored route) for the cinnamaldehyde hydrogenation (CAL). (In green dashed line circle: adsorptive CAL and hydroxyl could spatially interact to form a dynamic intermediate state through p−p overlapping of O atoms at the nanoscale interface of Pt/TiO_2, which leads to electron redistribution and accelerates C=O bond cleavage and consequently accelerates the reduction of CAL.)

Conclusion

In summary, just by simply tuning the interfacial microenvironment of catalytic active site of Pt@P25 catalysts with the selective adsorption of organic additives, the selective transformation of C=C and C=O groups of cinnamaldehyde (CAL) was achieved. We demonstrate that, the catalytic performance of selective hydrogenation of CAL is strongly dependent on the nature of interface states, rather than the crystal structure of titania (TiO_2). As-made and sodium formate (HCOONa) adsorbed Pt@P25 catalysts exhibit the preferred hydrogenation of C=C double bonds, i.e, the production of HCAL, owing to the blocking of Pt active sites by the spontaneously formed interfacial carbonate species and formate anions, which suppresses the adsorption of C=O groups of CAL. In the basic solution (CH_3ONa and NaOH), due to the competitive binding of hydroxide groups (OH^-) on carbonate or organic species at Pt surface, a new surface state in the form of hydrated hydroxide complex is produced though space overlapping of p orbitals of O atoms, which promote the favorite interaction of C=O groups of CAL, preferentially resulting in the production of COL. This investigation indicated that the reconstruction or restructuring of surface states with mimic microenvironment of metal enzymes is an efficient strategy to regulate the selective chemical transformations for a family of α, β-unsaturated aldehydes at heterogeneous metal naoscale interfaces.

Author Contributions: RT and BQS equally contribute to this research, HDS and MD performed part of experiments. KZ conceived and directed the project. KZ and BQS analyzed all the data and co-designed the figures with the help of QSX, JGJ and PW. KZ and BOS wrote the manuscript with the help of PW. All authors have read and agreed to the published version of the manuscript.

Acknowledgments: This research was funded by the NSFC (21872053 and 21573074), the Science and Technology Commission of Shanghai Municipality (19520711400) and the CAS key laboratory of Low-Coal Conversion Science & Engineering (KLLCCSE-201702), and the JORISS program.

Reference

1. P. Gallezot, D. Richard, Selective Hydrogenation of α,β-Unsaturated Aldehydes. *Catal. Rev.* **40**, 81-126 (1998).
2. P. Mäki-Arvela, J. Hájek, T. Salmi, D. Y. Murzin, Chemoselective hydrogenation of carbonyl compounds over heterogeneous catalysts. *Appl. Catal. A: Gen.* **292**, 1-49 (2005).
3. L. Liu, A. Corma, Metal Catalysts for Heterogeneous Catalysis: From Single Atoms to Nanoclusters and Nanoparticles. *Chem. Rev.* **118**, 4981-5079 (2018).
4. C. Xie, Z. Niu, D. Kim, M. Li, P. Yang, Surface and Interface Control in Nanoparticle Catalysis. *Chem. Rev.* **120**, 1184-1249 (2020).
5. M. Luneau *et al.*, Guidelines to Achieving High Selectivity for the Hydrogenation of alpha,beta-Unsaturated Aldehydes with Bimetallic and Dilute Alloy Catalysts: A Review. *Chem. Rev.* **120**, 12834-12872 (2020).
6. J. Zhang *et al.*, Origin of synergistic effects in bicomponent cobalt oxide-platinum catalysts for selective hydrogenation reaction. *Nat. Commun.* **10**, 4166 (2019).
7. J. M. Thomas, R. J. Williams, Catalysis: principles, progress, prospects. *Philos. Trans. R. Soc. A* **363**, 765-791; discussion 1035-1040 (2005).
8. K. R. Kahsar, D. K. Schwartz, J. W. Medlin, Control of metal catalyst selectivity through specific noncovalent molecular interactions. *J. Am. Chem. Soc.* **136**, 520-526 (2013).
9. K. R. Kahsar, D. K. Schwartz, J. W. Medlin, Selective Hydrogenation of Polyunsaturated Fatty Acids Using Alkanethiol Self-Assembled Monolayer-Coated Pd/Al2O3 Catalysts. *ACS Catal.* **3**, 2041-2044 (2013).
10. C. A. Schoenbaum, D. K. Schwartz, J. W. Medlin, Controlling the surface environment of heterogeneous catalysts using self-assembled monolayers. *Acc. Chem. Res.* **47**, 1438-1445 (2014).
11. M. Zhao *et al.*, Metal-organic frameworks as selectivity regulators for hydrogenation reactions. *Nature* **539**, 76-80 (2016).
12. L. Altmann, S. Kunz, M. Bäumer, Influence of Organic Amino and Thiol Ligands on the Geometric and Electronic Surface Properties of Colloidally Prepared Platinum Nanoparticles. *J. Phys. Chem. C* **118**, 8925-8932 (2014).
13. Y. Lou *et al.*, Pocketlike Active Site of Rh1/MoS2 Single-Atom Catalyst for Selective Crotonaldehyde Hydrogenation. *J. Am. Chem. Soc.* **141**, 19289–19295 (2019).
14. M. Khan, S. Joshi, V. Ranade, Kinetics of cinnamaldehyde hydrogenation in four phase system. *Chem. Eng. J.* **377**, 120512-120520 (2019).
15. Y. Li *et al.*, Solvent effects on heterogeneous catalysis in the selective hydrogenation of cinnamaldehyde over a conventional Pd/C catalyst. *Catal. Sci. Technol.* **8**, 3580-3589 (2018).
16. K. Liu, R. Qin, N. Zheng, Insights into the Interfacial Effects in Heterogeneous Metal Nanocatalysts toward Selective Hydrogenation. *J. Am. Chem. Soc.* **143**, 4483-4499 (2021).
17. Y. Wang *et al.*, Chemoselective Hydrogenation of Nitroaromatics at the Nanoscale Iron(III)-OH-Platinum Interface. *Angew. Chem. Int. Ed.* **59**, 12736-12740 (2020).
18. B. Wu, H. Huang, J. Yang, N. Zheng, G. Fu, Selective hydrogenation of alpha,beta-unsaturated aldehydes catalyzed by amine-capped platinum-cobalt nanocrystals. *Angew. Chem. Int. Ed.* **51**, 3440-3443 (2012).

19. P. Liu. *et al.*, Photochemical route for synthesizing atomically dispersed palladium catalysts. *Science* **352**, 797-801 (2016).
20. G. Chen *et al.*, Interfacial electronic effects control the reaction selectivity of platinum catalysts. *Nat. Mater.* **15**, 564-569 (2016).
21. H. Zhou. *et al.*, Isolated boron in zeolite for oxidative dehydrogenation of propane. *science* **372**, 76–80 (2021).
22. L. Wang *et al.*, Single-site catalyst promoters accelerate metal-catalyzed nitroarene hydrogenation. *Nat. Commun.* **9**, 1362-1369 (2018).
23. J. Zhang *et al.*, A Pd@Zeolite Catalyst for Nitroarene Hydrogenation with High Product Selectivity by Sterically Controlled Adsorption in the Zeolite Micropores. *Angew. Chem. Int. Ed.* **56**, 9747-9751 (2017).
24. L. Wang *et al.*, Silica accelerates the selective hydrogenation of CO2 to methanol on cobalt catalysts. *Nat. Commun.* **11**, 1033 (2020).
25. L. Bonneviot, G. L. Haller, Morphology and site blocking effects on chemisorption properties and reactivity of Pt/TiO2 and sulfided Pt/Al2O3 catalysts. *J. Catal.* **20**, 359-373 (1991).
26. J. N. Kuhn, C.-K. Tsung, W. Huang, G. A. Somorjai, Effect of organic capping layers over monodisperse platinum nanoparticles upon activity for ethylene hydrogenation and carbon monoxide oxidation. *J Catal.* **265**, 209-215 (2009).
27. A. R. Riscoe *et al.*, Transition state and product diffusion control by polymer–nanocrystal hybrid catalysts. *Nat. Catal.* **2**, 852-863 (2019).
28. X. Ren *et al.*, Microenvironment Engineering of Ruthenium Nanoparticles Incorporated into Silica Nanoreactors for Enhanced Hydrogenations. *Angew. Chem. Int. Ed.* **58**, 14483-14488 (2019).
29. R. Gao *et al.*, Ultradispersed Nickel Phosphide on Phosphorus-Doped Carbon with Tailored d-Band Center for Efficient and Chemoselective Hydrogenation of Nitroarenes. *ACS Catal.* **8**, 8420-8429 (2018).
30. Y. Xiao *et al.*, Molecule Self-Assembly Synthesis of Porous Few-Layer Carbon Nitride for Highly Efficient Photoredox Catalysis. *J. Am. Chem. Soc.* **141**, 2508-2515 (2019).
31. H. Chen *et al.*, Sulfur dots-graphene nanohybrid: a metal-free electrocatalyst for efficient N2-to-NH3 fixation under ambient conditions. *Chem. Commun.* **55**, 3152-3155 (2019).
32. Y. Chen *et al.*, Photoemission mechanism of water-soluble silver nanoclusters: ligand-to-metal-metal charge transfer vs strong coupling between surface plasmon and emitters. *J. Am. Chem. Soc.* **136**, 1686-1689 (2014).
33. T. Yang *et al.*, Interfacial Clustering-Triggered Fluorescence-Phosphorescence Dual Solvoluminescence of Metal Nanoclusters. *J. Phys. Chem. Lett.* **8**, 3980-3985 (2017).
34. T. Yang *et al.*, Mechanism of Photoluminescence in Ag Nanoclusters: Metal-Centered Emission versus Synergistic Effect in Ligand-Centered Emission. *J. Phys. Chem. C* **123**, 18638-18645 (2019).
35. T. Yang *et al.*, P band intermediate state (PBIS) tailors photoluminescence emission at confined nanoscale interface. *Commun. Chem.* **2**, 132 (2019).
36. Y. Taiqun, P. Bo, Z. Jiafeng, S. Bingqian, Z. Kun, Hydrogen-Bonded Water Clusters Confined in Nanocavity as Bright Color Emitters. *ChemRxiv* (2020).
37. H. Xiao-Dan, Y. Taiqun, S. Bingqian, P. Bo, Z. Kun, Topological Excitation of Singly Hydrated Hydroxide Complex in Confined Sub-Nanospace for Bright Color Emission and Heterogeneous

Catalysis. *ChemRxiv* (2020).

38. T. Q. Yang *et al.*, Origin of the Photoluminescence of Metal Nanoclusters: From Metal-Centered Emission to Ligand-Centered Emission. *Nanomaterials (Basel)* **10**, 261 (2020).
39. T.-Q. Yang *et al.*, Interfacial electron transfer promotes photo-catalytic reduction of 4-nitrophenol by Au/Ag2O nanoparticles confined in dendritic mesoporous silica nanospheres. *Catal. Sci. Technol.* **9**, 5786-5792 (2019).
40. X.-D. Hu, B.-Q. Shan, R. Tao, T.-Q. Yang, K. Zhang, Interfacial Hydroxyl Promotes the Reduction of 4-Nitrophenol by Ag-based Catalysts Confined in Dendritic Mesoporous Silica Nanospheres. *J. Phys. Chem. C* **125**, 2446−2453 (2021).
41. B.-Q. Shan, J.-F. Zhou, M. Ding, X.-D. Hu, K. Zhang, Surface Electronic State Mediates Proton Transfer at Metal Nanoscale Interface for Catalytic Hydride Reduction of −NO2 to −NH2. *ChemRxiv* (2021).
42. Jan Balajka *et al.*, High-affinity adsorption leads to molecularly ordered interfaces on TiO2 in air and solution. *science* **361**, 786–789 (2019).
43. A. Song, E. S. Skibinski, W. J. I. DeBenedetti, A. G. Ortoll-Bloch, M. A. Hines, Nanoscale Solvation Leads to Spontaneous Formation of a Bicarbonate Monolayer on Rutile (110) under Ambient Conditions: Implications for CO2 Photoreduction. *J. Phys. Chem. C* **120**, 9326-9333 (2016).
44. B. Bachiller-Baeza, Rodriguez-Ramos, A. Guerrero-Ruiz, Interaction of Carbon Dioxide with the Surface of Zirconia Polymorphs. *Langmuir* **14**, 3556-3564 (1998).
45. W. Su *et al.*, Surface Phases of TiO2 Nanoparticles Studied by UV Raman Spectroscopy and FT-IR Spectroscopy. *J. Phys. Chem. C* **11**, 7710–7716 (2008).
46. G. Martra, Lewis acid and base sites at the surface of microcrystalline TiO2 anatase: relationships between surface morphology and chemical behaviour. *Appl. Catal. A: Gen.* **200**, 275–285 (2000).
47. Ming-Yuan He, J. M. WHITE, CO and CO2 hydrogenation over metal oxides a comparison of ZnO, TiO2 and ZrO2. *J. Mol. Catal.* **30**, 415-430 (1985).
48. H. Doghri, E. A. Baranova, B. Albela, M. Saïd-Zina, L. Bonneviot, A bio-inspired zinc finger analogue anchored in 2D hexagonal mesoporous silica for room temperature CO2 activation via a hydrogenocarbonate route. *New J. Chem.* **41**, 6795-6809 (2017).
49. J. Peng *et al.*, Surface coordination layer passivates oxidation of copper. *Nature* **586**, 390-394 (2020).
50. F. Scholz *et al.*, Crystal Structure Determination of the Nonclassical 2-Norbornyl Cation. *Science* **341**, 62 (2013).

Graphic abstract

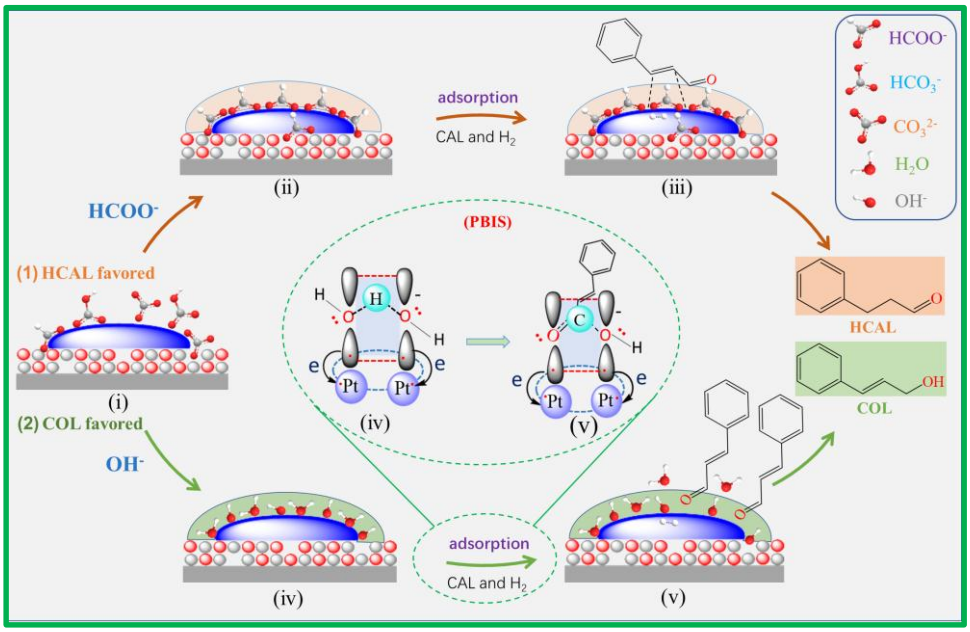

Surface molecule manipulated Pt/TiO2 catalysts for selective hydrogenation of cinnamaldehyde.

Supporting Information

Surface Molecule Manipulated Pt/TiO_2 Catalysts for Selective Hydrogenation of Cinnamaldehyde

Ran Tao, [1#] Bing-Qian Shan, [#*1] Hao-Di Sun,[1] Meng-Ding, [1] Qing-Song Xue,[1] Jin-Gang Jiang, [1] Peng Wu, [1*] Kun Zhang[1,2*]

[1] Shanghai Key Laboratory of Green Chemistry and Chemical Processes, Laboratory of Interface and Water Science, College of Chemistry and Molecular Engineering, East China Normal University, Shanghai 200062, China;

[2] Shandong Provincial Key Laboratory of Chemical Energy Storage and Novel Cell Technology, School of Chemistry and Chemical Engineering, Liaocheng University, Liaocheng, 252059, Shandong, P. R. China.

*Correspondence:bqshan_ecnu@163.com, kzhang@chem.ecnu.edu.cn, pwu@chem.ecnu.edu.cn

Table of Contents

Experiment section

Materials

Chloroplatinic acid (H_2PtCl_6, 37 wt% Pt), sodium borohydride ($NaBH_4$, 98%), ethanol (EtOH, 99.7%) were purchased from Sinopharm (China). P25 were provided by Acros origanics. Cinnamyl aldehyde (CAL, 98%) were obtained from Aladdin Industrial Corporation. All the chemicals were used without further purification.

Techniques

The X-ray diffraction (XRD) patterns were required using a Rigaku Ultima Discover X-Ray Diffractometer at a wavelength of Cu Kα (1.5405 Å). The SEM and TEM images were taken using Hitachi S-4800 microscope and JEOL-JEM-2100 microscope, respectively. FT-IR spectra were recorded by Nicolet Fourier transform infrared spectrometer (NEXUS 670) using the KBr technique. Thermogravimetric analysis (TG) was performed on a Mettler TGA/SDTA 851e instrument with a heating rate of 10℃ / min under an air flow. Gas chromatographic mass spectrometry were analyzed and quantified by Agilent HP6890/5973N.

Synthesis of Pt@P25-T (T=270, 500, 700℃) catalysts

H_2PtCl_6 $6H_2O$ aqueous (6.635 mL, 7.72 mM), 40 mL of ethanol and 0.5 g of P25 were mixed together and stirred for 12 h at room temperature, and then 40 mg $NaBH_4$ was introduced. After stirring 30 min, the suspension was filtered and washed with water and ethanol, and drying at 80℃. After impregnation, the sample were calcinated at 270℃, 500℃ and 700℃ for 2 h in air. The as-obtained samples were denoted as Pt@P25-T (T=270, 500, 700℃). The calculated Pt content was 2 wt%.

Synthesis of Pt@(P25-T) (T=270, 500, 700℃) catalysts

P25 was transferred into the crucible and followed by the calcination at various temperatures (270℃, 500℃ and 700℃) in a muffle furnace for 2 h. H_2PtCl_6 $6H_2O$ aqueous (6.635 mL, 7.72 mM), 40 mL of ethanol and 0.5 g of P25-T were mixed together and stirred for 12 h at room temperature, and then 40 mg $NaBH_4$ was introduced. After stirring 30 min, the suspension was filtered and washed with water and ethanol, and drying at 80℃. The as-obtained samples were denoted as Pt@(P25-T) (T=270, 500, 700).

Hydrogenation of cinnamaldehyde (CAL)

CAL hydrogenation reactions were performed on the above catalysts in a stainless-steel autoclave reactor. The reaction was carried out at 60 ℃ and 2.0 MPa H_2 with a certain amount of catalysts in 4 mL of ethanol, 0.4mL of H_2O, 0.1 mL of CAL and 23 mg catalyst. After the reaction, the reactor was cooled and then slowly depressurized. Finally, the reaction mixture was separated by centrifugation in order to remove the solid catalysts. The reaction products were analyzed and quantified by gas chromatographic mass spectrometry (GC-MS, Agilent HP6890/5973N). The reaction conversion and selectivity were determined by the product analysis.

Experiment results

Table 1 | the physicochemical properties of Pt@P25-T and Pt@(P25-T) samples.

Sample	W_A[a] (%)	W_R[a] (%)	W_A/W_R	S_{BET}[b] (m^2/g)	Pore volume[c] (cm^3/g)	Pore size[d] (nm)
Pt@P25	80.4	19.6	4.1	42.9	0.91	75.3
Pt@P25-270	78.6	21.4	3.7	60.2	0.74	49.4
Pt@P25-500	78.5	21.5	3.7	37.3	0.41	44.1
Pt@P25-700	0	100	0	4.1	0.03	30.7
Pt@(P25-270)	80.4	19.6	4.1	47.1	0.80	68.0
Pt@(P25-500)	79.6	20.4	3.9	45.1	0.50	44.5
Pt@(P25-700)	41.9	58.1	0.7	22.4	0.25	44.6

[a] A and R denote as anatase and rutile, respectively. [b] Specific surface area measured from N_2 physisorption. [c] Total pore volume measured at P/P_0=0.99.
[d] The porosity is estimated from the pore volume determined using the desorption data.

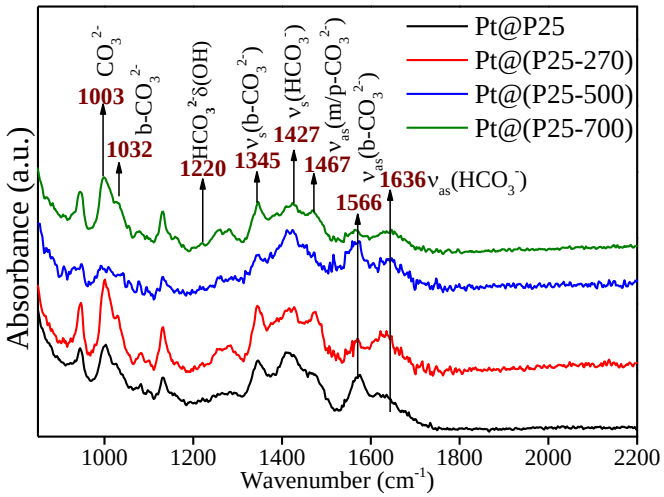

Fig S1. FT-IR spectra of Pt@(P25-T) (T= 270, 500, and 700℃).

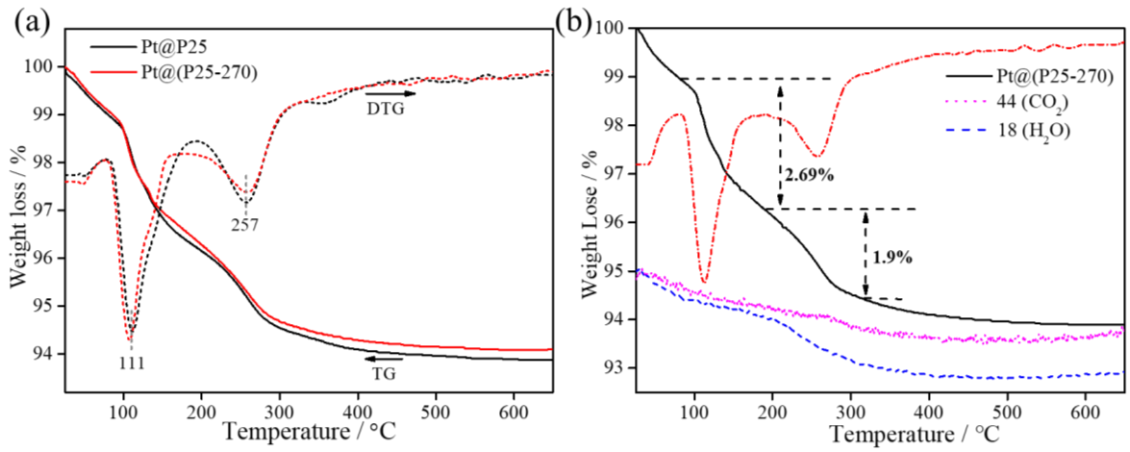

Fig S2. (a) TG-DTG analysis of Pt@P25 and Pt@(P25-270). (b) Thermo-gravimetricanalysis-Mass spectrum (TG-MAS) of Pt@(P25-270).

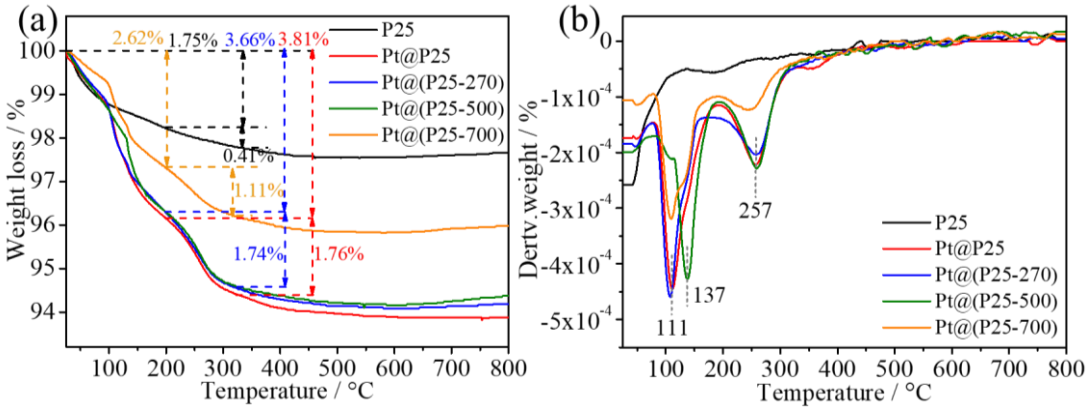

Fig S3. TG-DTG analysis of P25 and Pt@(P25-T) (T= room temperature, 270℃, 500℃, and 700℃).

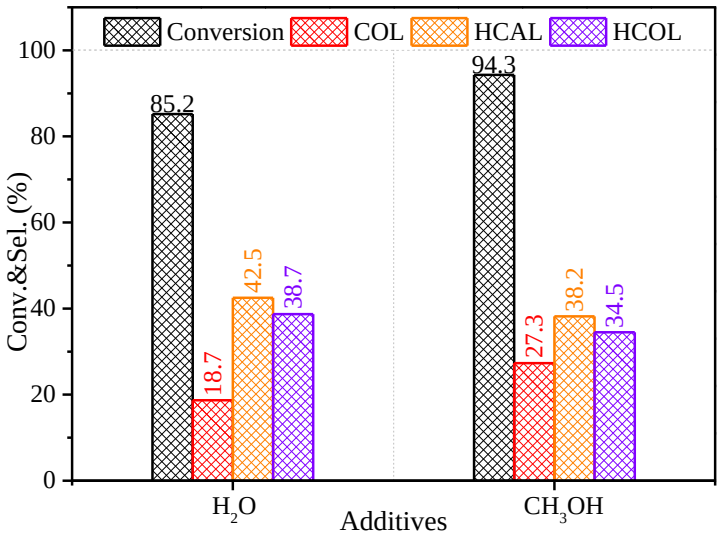

Fig S4. Selective hydrogenation of CAL at H_2O and CH_3OH with Pt@(P25-270).

Table 2 | Selective hydrogenation of cinnamyl aldehyde

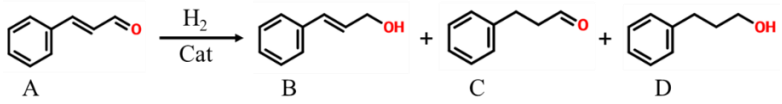

					Selectivity (%)		
Entry	Cat	Additives	pH	Conversion (%)	B	C	D
1	Pt@(P25-270)	H_2O	5.13	85.2	18.7	42.5	38.7
2	Pt@(P25-270)	CH_3COONa	8.25	94.6	80	9.9	10.4
3	Pt@(P25-270)	CH_3ONa	12.45	97.6	98.9	0.7	0.3
4	Pt@(P25-270)	NaOH	12.56	97.3	91.6	7.1	1.3
5	Pt@DMSNs	H_2O	6.75	86.8	25.9	49.6	24.5
6	Pt@DMSNs	NaOH	12.82	85.6	95.6	2.8	1.6

A, cinnamaldehyde (CAL); B, cinnamyl alcohol (COL); C, hydrocinnamaldehyde (HCAL); D, hydrocinnamyl alcohol (HCOL).
Reaction condition: catalyst (23mg), A (0.1 mL), ethanol (4.0 mL), H_2O (0.4 mL) or additives (1M, 0.4 mL), H_2 (2 MPa), T (60 ℃), t (1 h)
The percentage conversion of A and selectivity for specific products were determined by gas chromatography-mass spectrometry and gas chromatography

Table 3 | Infrared vibrational frequency correlation chart of interfacial carbonaceous species found in P25-Pt (*1-3*).

Species	Structure	Vibration mode	IR bands (cm^{-1})	Reference
Monodentate carbonate ($m\text{-}CO_3^{2-}$)	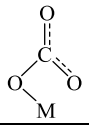	υ_s ($m\text{-}CO_3^{2-}$)	1382	(*1-3*)
		υ_{as} ($m\text{-}CO_3^{2-}$)	1468	
bidentate carbonate ($b\text{-}CO_3^{2-}$)	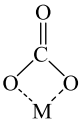		1032	(*1-3*)
		υ_s ($b\text{-}CO_3^{2-}$)	1345	
		υ_{as} ($b\text{-}CO_3^{2-}$)	1574	
bicarbonate (HCO_3^-)	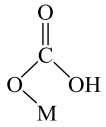	υ_s (HCO_3^-)	1427	(*1-3*)
		υ_s (HCO_3^-)*	1411	
		υ_{as} (HCO_3^-)	1636	
		δ(OH)	1220	
Carboxylate (COO^-)		υ_s (COO^-)	1271	(*1*)
		υ_{as} (COO^-)	1690	
Non-classical carbon species	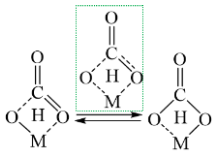		1440	**This work** and (*4*)
			1557	
			1675	

* HCO_3^- absorbed on anatase

Reference

1. W. Su *et al.*, Surface Phases of TiO2 Nanoparticles Studied by UV Raman Spectroscopy and FT-IR Spectroscopy. *J. Phys. Chem. C* **11**, 7710–7716 (2008).

2. G. Martra, Lewis acid and base sites at the surface of microcrystalline TiO2 anatase: relationships between surface morphology and chemical behaviour. *Appl. Catal. A: Gen.* **200**, 275–285 (2000).

3. B. Bachiller-Baeza, Rodriguez-Ramos, A. Guerrero-Ruiz, Interaction of Carbon Dioxide with the Surface of Zirconia Polymorphs. *Langmuir* **14**, 3556-3564 (1998).

4. F. Scholz *et al.*, Crystal Structure Determination of the Nonclassical 2-Norbornyl Cation. *Science* **341**, 62 (2013).